





















## Synthesis of the land carbon fluxes of the Amazon region between 2010 and 2020

Thais M. Rosan <sup>1✉</sup>, Stephen Sitch <sup>1</sup>, Michael O'Sullivan<sup>1</sup>, Luana S. Basso <sup>2,3</sup>, Chris Wilson <sup>4,5</sup>, Camila Silva<sup>6,7,8</sup>, Emanuel Gloor<sup>2</sup>, Dominic Fawcett<sup>1,9</sup>, Viola Heinrich<sup>1</sup>, Jefferson G. Souza<sup>1</sup>, Francisco Gilney Silva Bezerra <sup>3</sup>, Celso von Randow<sup>3</sup>, Lina M. Mercado <sup>1,10</sup>, Luciana Gatti <sup>3</sup>, Andy Wiltshire<sup>1,11</sup>, Pierre Friedlingstein <sup>1</sup>, Julia Pongratz<sup>12,13</sup>, Clemens Schwingshackl <sup>12</sup>, Mathew Williams <sup>14</sup>, Luke Smallman<sup>14</sup>, Jürgen Knauer <sup>15</sup>, Vivek Arora<sup>16</sup>, Daniel Kennedy<sup>17</sup>, Hanqin Tian <sup>18</sup>, Wenping Yuan <sup>19</sup>, Atul K. Jain <sup>20</sup>, Stefanie Falk<sup>12</sup>, Benjamin Poulter <sup>21</sup>, Almut Arneth<sup>22</sup>, Qing Sun <sup>23</sup>, Sönke Zaehle<sup>24</sup>, Anthony P. Walker<sup>25</sup>, Etsushi Kato<sup>26</sup>, Xu Yue <sup>27</sup>, Ana Bastos <sup>24</sup>, Philippe Ciais <sup>28</sup>, Jean-Pierre Wigneron <sup>29</sup>, Clement Albergel<sup>30</sup> & Luiz E. O. C. Aragão<sup>1,3</sup>

The Amazon is the largest continuous tropical forest in the world and plays a key role in the global carbon cycle. Human-induced disturbances and climate change have impacted the Amazon carbon balance. Here we conduct a comprehensive synthesis of existing state-of-the-art estimates of the contemporary land carbon fluxes in the Amazon using a set of bottom-up methods (i.e., dynamic vegetation models and bookkeeping models) and a top-down inversion (atmospheric inversion model) over the Brazilian Amazon and the whole Biogeographical Amazon domain. Over the whole biogeographical Amazon region bottom-up methodologies suggest a small average carbon sink over 2010-2020, in contrast to a small carbon source simulated by top-down inversion (2010-2018). However, these estimates are not significantly different from one another when accounting for their large individual uncertainties, highlighting remaining knowledge gaps, and the urgent need to reduce such uncertainties. Nevertheless, both methodologies agreed that the Brazilian Amazon has been a net carbon source during recent climate extremes and that the south-eastern Amazon was a net land carbon source over the whole study period (2010-2020). Overall, our results point to increasing human-induced disturbances (deforestation and forest degradation by wildfires) and reduction in the old-growth forest sink during drought.

The Amazon covers an area of ~7 million km<sup>2</sup> and accounts for about 40% of global tropical forest area, storing around 229–280 Pg C (Petagram of carbon) in living biomass and dead organic matter in soils<sup>1,2</sup>, of which approximately 108 (95% CI 101–115) Pg C is aboveground in live trees<sup>3</sup>. As a result, the Amazon forest plays a key role in the global carbon cycle and even small perturbations, as a consequence of human disturbances<sup>4</sup> and climate change, can have an impact on global climate<sup>5,6</sup>, as well as on South America's hydrological cycle<sup>7</sup>. The carbon sink contribution of the old-growth forests (i.e., forests not impacted by contemporary human-induced disturbances) in the Amazon has been estimated to be undergoing a persistent decline, driven by an increase in tree mortality, associated with environmental change<sup>8–11</sup>. The old-growth Amazon forest may thus continue to lose its climate change mitigation role by absorbing less carbon from the atmosphere in the future<sup>8–11</sup>.

Alongside the effects of environmental change, in particular the increasing concentration of CO<sub>2</sub> in the atmosphere driven by anthropogenic activities, the Amazon has also been impacted by human-induced disturbances. These disturbances are caused by large-scale land use and land cover changes (LULCC) and landscape fragmentation driven by deforestation, and extensive forest degradation through wildfires caused by anthropogenic activity in association to drier conditions and logging. These human-induced disturbances resulted in aboveground carbon (AGC) losses of 1.3 (±0.4) Pg C between 2012 and 2019<sup>12</sup>. After reaching the lowest deforestation rate in 2012, the Brazilian Amazon suffered an upturn with consistent intensification of deforestation rates<sup>13</sup>. This pattern shift in deforestation caused an increase of about 140% in CO<sub>2</sub> emissions in 2020 compared to the decadal low in 2012<sup>14</sup>. Moreover, the areal extent and gross carbon emissions from forest degradation can even exceed those from deforestation, especially in extreme drought years<sup>15–19</sup>. Forest degradation through fire reduces the potential of secondary forests to accumulate carbon<sup>20</sup> and regrowing burned Amazon humid forests are not able to offset the initial disturbance emissions even 30 years after the fire occurrence<sup>21</sup>. Other processes such as logging and edge effects induced by landscape fragmentation result in additional carbon losses and subsequent carbon emissions to the atmosphere<sup>12,22</sup>. When taken together, these disturbance processes increase the carbon sources impeding their offset by the carbon sink in old-growth forests, which shows evidence of a decline<sup>8</sup> therefore, shifting the net carbon balance of the Amazon towards (higher) emissions to the atmosphere.

There are multiple approaches to estimate the land carbon fluxes. Bottom-up approaches comprise the use of process-based Dynamic Global Vegetation Models (DGVMs)<sup>23</sup> and bookkeeping models<sup>24–26</sup>, as well as remote sensing-based estimates<sup>27</sup>. Top-down approaches are based on atmospheric inversion models, which combine in situ CO<sub>2</sub> measurements, aircraft measurements of CO<sub>2</sub> concentration and atmospheric transport model simulations<sup>28</sup>. There are discrepancies between bottom-up and top-down estimates for the South America carbon budget, with the top-down inversions estimating a net land source and bottom-up a net land sink<sup>29</sup>. Studies of Amazon carbon fluxes have concentrated mostly on the roles of old-growth forests as a carbon sink<sup>8</sup>, on the emissions from deforestation and forest degradation<sup>27,30,31</sup>, or on net biome productivity (NBP)<sup>32,33</sup>. They use different methodologies, study periods, and spatial domains of the Amazon area (e.g., whole Amazon vs Brazilian Amazon) which causes difficulties in comparing estimates. The Brazilian Amazon forests were estimated to be a net carbon source of +0.06 (−0.01 to +0.31) Pg C yr<sup>−1</sup> in 2010 based on a literature review and compilation of datasets<sup>33</sup>. Estimates based on Earth observation data focusing on the carbon gains and losses

in forest areas derived from the Global Forest change product<sup>34</sup> and using emissions and removal factors from the Intergovernmental Panel on Climate Change (IPCC) guidelines, indicated that the whole Amazon Forest region was a net carbon sink between 2001 and 2019, while the Brazilian part of the Amazon forest acted as a net carbon source as a result of deforestation<sup>27</sup>. A study using in situ observations of gases (e.g., CO and CO<sub>2</sub>) by aircraft-borne flasks and an atmospheric transport inverse modelling approach concluded that the Amazon region was a small net carbon source over the 2010–2018 period, driven mostly by fire emissions from the south-east Amazon region<sup>32</sup>.

Knowledge gaps remain about the processes included in bottom-up models (e.g., anthropogenic wildfires and fire and drought-induced tree mortality<sup>21,35</sup>), the land use and land cover change data used in these model simulations<sup>36</sup>, as well as consistent uncertainty estimates. Therefore, a synthesis and standardization of existing estimates of the net land carbon fluxes of the Amazon region is needed to characterize the contemporary state of the net land carbon fluxes, and to clarify where the main gaps remain to reconcile differences of flux estimates between top-down and bottom-up approaches. Given the importance of the Amazon for the global carbon cycle and the recent changes in deforestation pattern, the main aim of this study is to provide a comprehensive state-of-the-art synthesis of the net land-atmosphere carbon flux of the whole Amazon as well as the Brazilian Amazon area for the 2010–2020 period.

Here we quantify the net land carbon fluxes of the whole biogeographical domain of the Amazon<sup>37</sup> and of the Brazilian Amazon, using existing data from top-down atmospheric transport inversion<sup>38</sup>, and a combination of bottom-up model-based estimates<sup>26,30,39</sup>. To estimate the net carbon sources from human-induced forest disturbances, we use a set of bottom-up estimates of disturbance fluxes including deforestation and forest degradation and subsequent regrowth using regional<sup>26,30</sup> and global spatially explicit bookkeeping models<sup>25,39,40</sup>. These bookkeeping models are constrained with satellite estimates of deforestation and degradation area and use response curves of decomposition and tree growth to estimate the resulting net carbon fluxes caused by deforestation and degradation (see further detail of each model in the Methods section). To estimate the net carbon sink of old-growth forests, we use a set of Dynamic Global Vegetation Models (DGVMs) which participated in the Global Carbon Budget 2022 (GCB)<sup>39</sup> assessment, called TRENDY-v11. We then combine all estimates of net sources and sinks from the bottom-up models to calculate the spatiotemporal net land carbon fluxes for the whole Biogeographical Amazon and for the Brazilian Amazon, separately (see domain limits in Supplementary Fig. 1 and model combinations in Table 3 of Methods section). Finally, we synthesize and present the net land carbon fluxes based on the bookkeeping models combination with TRENDY-v11 DGVMs (bottom-up estimates), the bottom-up net flux estimate from the CARDAMOM model-data fusion framework<sup>41,42</sup> and top-down atmospheric inversion estimates (TOMCAT) using a global atmospheric transport model<sup>38</sup> that is constrained with atmospheric profile measurements<sup>32</sup>. Figure 1 shows an overview of the methodologies used to estimate the carbon fluxes of each domain. Note that the model combination used to calculate the net land carbon fluxes with bookkeeping models and TRENDY-v11 DGVMs differs between the whole Biogeographical Amazon and Brazilian Amazon due to differences in data availability for each region as described in Table 3 in the methods section. Hereafter we adopt a + sign convention to represent a net flux of carbon from land to the atmosphere (source) and a - sign convention for a net carbon flux into the land (sink).

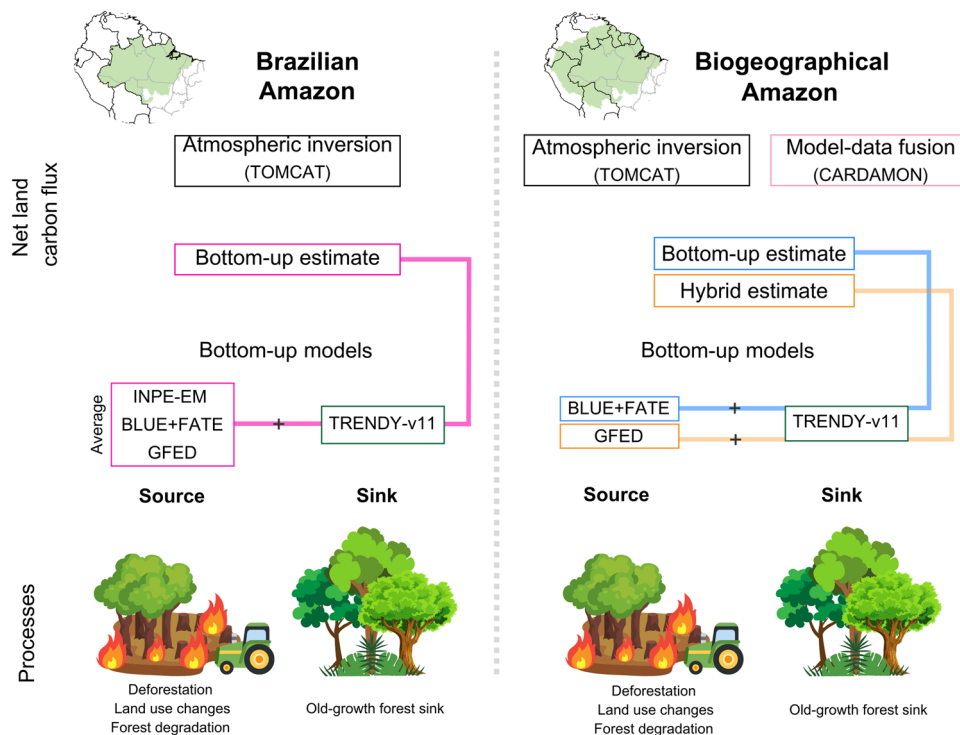


**Fig. 1 Overview of the existing methodologies applied to estimate the carbon fluxes in the Brazilian Amazon and Biogeographical Amazon according to data availability.** Details of each bookkeeping models (INPE-EM, BLUE, FATE and GFED), TRENDY-v11 DGVMs, TOMCAT atmospheric inversion (called top-down inversion in the results section) and CARDAMON can be found in the methods section and their combinations in Table 3. Further detailed information about the processes included in each model can be found in Table 2 and Supplementary Table 3 for the TRENDY-v11 DGVMs.

## Results

**Spatiotemporal attribution of the land carbon fluxes in the whole biogeographical Amazon.** For the whole biogeographical Amazon, we relied on two global models to estimate the disturbance flux. A combination of net land use flux estimates from the Bookkeeping of Land Use Emissions (BLUE) added to the net wildfire flux from a fire bookkeeping model (FATE) (BLUE + FATE, see Methods), suggests the whole biogeographical Amazon released a net flux of  $192 \text{ Tg C yr}^{-1}$  over 2010–2020 to the atmosphere from land use and land cover changes and forest degradation fires. Over the same period, the Global Fire Emissions Database (GFED) suggested an average flux of  $89 \text{ Tg C yr}^{-1}$  from deforestation and degradation fires (Table 1). Both BLUE + FATE and GFED show similar interannual variability (Fig. 2a). However, the average flux simulated by BLUE + FATE is 116% higher than GFED, as the former includes more processes linked to land use and land cover changes, such as fluxes from transitions between different land uses, shifting cultivation, soil carbon and legacy fluxes, as well as the addition of the net legacy fluxes of forest degradation by fire from the FATE model, which include late tree mortality by fire. The GFED estimates used here only account for biomass burning flux from tropical forest fires linked to deforestation and degradation but assume that degraded forests are carbon neutral (i.e., GFED does not include late tree mortality fluxes). Spatially, both models show that most of the net disturbance fluxes are concentrated in the south-eastern Amazon region (i.e., in the Southern Brazilian Amazon) (Fig. 2c, d). As none of the two models used to estimate the disturbance flux for the whole Biogeographical Amazon provides regional uncertainty estimates, we are unable to quantify the uncertainty for the disturbance term.

The average old-growth forest sink simulated by TRENDY-v11 DGVMs (16 models) for the whole biogeographical Amazon was

$-333 (\pm 195) \text{ Tg C yr}^{-1}$  over the 2010–2020 period (Table 1). The old-growth forest sink shows a high interannual variability driven by intense drought events which causes a water stress in the vegetation<sup>43</sup> and is associated with the El Niño–Southern Oscillation (ENSO) years over our study period ( $R = -0.6$ ;  $p = 0.051$  in Supplementary Fig. 2c). Those drought events reduce the sink capacity of these forests in our estimates due to the reduced simulated productivity in the DGVMs (e.g., 2015/2016 in Fig. 2b). Spatially, the average old-growth forest sink was higher in the western and northern parts of the Amazon (Fig. 2e) where most of the old-growth forest is located. Lower values occur across the south-eastern regions along the areas with lower intact old-growth forest percentage due to deforestation and degradation (see the fraction mask of old-growth forests applied to the DGVMs in Supplementary Fig. 5). Stronger patterns in the old-growth forest sink, such as the pink grid-cells in Fig. 2e, are driven by lower annual precipitation ( $<1000 \text{ mm}$ ) during the 2015/2016 ENSO in the precipitation data used as input in the TRENDY-v11 DGVMs (Supplementary Fig. 3). Several DGVMs simulate a stronger transition of the old-growth forest from sink to source in this region in 2015/2016, which dominates the decadal mean flux (Supplementary Figure 4). This localized pattern points to the general sparsity of climate datasets across this important region for interpolation in reanalysis datasets, which are used as input for the DGVMs simulations.

Between 2010 and 2015 the old-growth forest sink based on field data from the Amazon Forest Inventory Network (RAINFOR) upscaled to the Amazon was  $-271 (\text{CI } 0.00\text{--}502) \text{ Tg C yr}^{-1}$ <sup>9,44</sup>. The old-growth forest sink simulated by TRENDY-v11 DGVMs was 26% larger than RAINFOR over the same period (average of  $-348 \pm 167 \text{ Tg C yr}^{-1}$ ). Although there is a difference in magnitude between the TRENDY DGVMs and the RAINFOR intact sink, they are not statistically significantly different over

**Table 1 Summary table with the average ( $Tg\ C\ yr^{-1} \pm 1\ SD$ ) carbon fluxes within the Brazilian Amazon and biogeographical Amazon over a common period (2010–2018).**

<b>Brazilian Amazon</b>				
	<b>2010–2018</b>	<b>2019</b>	<b>2020</b>	<b>2010–2020</b>
Disturbances bottom-up (Multi-model average)	+114 ( $\pm 67$ )	+129 ( $\pm 90$ )	+110 ( $\pm 54$ )	+115 ( $\pm 68$ )
Old-growth forest sink (TRENDY-v11)	–173 ( $\pm 141$ )	–219 ( $\pm 163$ )	–99 ( $\pm 156$ )	–170 ( $\pm 144$ )
<b>Net land carbon fluxes (Bottom-up)<sup>a</sup></b>	<b>–59 (<math>\pm 160</math>)</b>	<b>–91 (<math>\pm 186</math>)</b>	<b>+12 (<math>\pm 165</math>)</b>	<b>–55 (163)</b>
<b>Net land carbon fluxes (Top-down inversion)</b>	<b>36 (<math>\pm 125</math>)</b>	–	–	–
<b>Biogeographical Amazon</b>				
	<b>2010–2018</b>	<b>2019</b>	<b>2020</b>	<b>2010–2020</b>
Disturbances bottom-up (BLUE $E_{LUC}$ + FATE degradation fires)	+190	+221	+161	+192
Disturbances hybrid (GFED deforestation and degradation fires)	+86	+99	+107	+89
Old-growth forest sink (TRENDY-v11)	–342 ( $\pm 192$ )	–343 ( $\pm 212$ )	–239 ( $\pm 204$ )	–333 ( $\pm 195$ )
<b>Net land carbon fluxes (Bottom-up)</b>	<b>–152 (<math>\pm 192</math>)</b>	<b>–111 (<math>\pm 212</math>)</b>	<b>–66 (<math>\pm 204</math>)</b>	<b>–141 (<math>\pm 195</math>)</b>
<b>Net land carbon fluxes (Hybrid)</b>	<b>–255 (<math>\pm 192</math>)</b>	<b>–245 (<math>\pm 212</math>)</b>	<b>–131 (<math>\pm 204</math>)</b>	<b>–243 (<math>\pm 195</math>)</b>
<b>Net land carbon fluxes (CARDAMOM)</b>	<b>–339</b>	<b>–444</b>	<b>–266</b>	<b>–342</b>
<b>Net land carbon fluxes (Top-down inversion)</b>	<b>(CI –2945 – 2452)</b>	<b>(CI –2621 – 1587)</b>	<b>(CI –2366 – 1666)</b>	<b>(CI –2863 – 2287)</b>
<b>Net land carbon fluxes (Top-down inversion)</b>	<b>+27 (<math>\pm 130</math>)</b>	–	–	–

Estimates for 2019, 2020 and the average over 2010–2020 are provided separately subject to the availability of data. Individual disturbance models do not provide regional uncertainty estimates for the biogeographical Amazon. Therefore, the net land carbon flux uncertainty for the whole biogeographical Amazon is based only on the TRENDY-v11 old-growth sink uncertainty. Uncertainty estimates for CARDAMOM are provided as 95% confidence interval (CI). Further details about the single models and approaches can be found in the methods section (Table 3).

<sup>a</sup>The net land carbon fluxes are highlighted in bold.

this period ( $p = 0.37$ ; Supplementary Fig. 8). We also compared the aboveground carbon (AGC) change in intact areas between the TRENDY-v11 multi-model mean and AGC derived from satellite data from the L-Band Vegetation Optical Depth (L-VOD) from a recent study<sup>12</sup>. Although L-VOD based AGC shows an average net loss of carbon to the atmosphere of about  $35\ Tg\ C\ yr^{-1}$  and TRENDY-v11 AGC an average net carbon gain to the land of  $26\ Tg\ C\ yr^{-1}$  over the period of 2011–2019, a Welch's  $t$  test shows that their average values over this common period are not significantly different ( $p = 0.5$ ; Supplementary Fig. 9). Note that these values need to be compared cautiously due to potential differences in their old-growth forest mask and Amazon area, as well as in the processes included.

**Spatiotemporal attribution of the land carbon fluxes in the Brazilian Amazon.** A three-model combination that provides the net fluxes of forest disturbances (deforestation + degradation, including regrowth of these processes) was used to calculate one average estimate of the net disturbance flux (see Table 3 in Methods). We combine these three anthropogenic disturbances estimates due to the availability of regional estimates based on the official deforestation data from the Brazilian Amazon Monitoring Program (PRODES), as well as to be able to provide an estimate of the spread (uncertainty) for the Brazilian Amazon anthropogenic disturbance fluxes. The results show that the Brazilian Amazon released an average net flux of  $115\ Tg\ C\ yr^{-1}$  ( $\pm 68$ ; 1 SD multi-model range) to the atmosphere from all forest disturbances between 2010 and 2020 (Fig. 3a, black line). The multi-model mean net disturbance flux (Fig. 3a, black line) shows emission peaks in 2010, 2015 and an increased flux after 2018. The differences in the magnitude of individual disturbance models used to calculate the average disturbance flux for the Brazilian Amazon are due to the processes included and different driving data (see Methods section and Table 3 for further details of the main processes included in each model). Spatially, the disturbance fluxes are concentrated in the 'arc of deforestation' region in the southern Brazilian Amazon and along major roads that facilitate the advance of deforestation and spread of fires into forest edges (Fig. 3c).

Annual estimates of old-growth forest cover loss from the Brazilian Amazon Monitoring Program of the Instituto Nacional de Pesquisas Espaciais (PRODES/INPE) show that 2020 had the highest deforestation area in old-growth forest in the last decade<sup>13</sup>. This large area of deforestation in 2020 led to an increase of 12% (from  $68\ Tg\ C$  to  $76\ Tg\ C$ ) in the emissions estimated by the INPE emission model (INPE-EM) compared to 2019<sup>45</sup>. Yet, the multi-model disturbance average (black line in Fig. 3a) did not reproduce higher emissions in 2020 compared to 2019, which is due to the BLUE and GFED models showing a decrease in emissions between these two years (blue and orange lines in Fig. 3a). The reason for the diverging results between INPE-EM and the other two models is because they use different driving data and mapping calendar (see Methods for detailed information). The INPE-EM uses the Brazilian official deforestation dataset (PRODES/INPE) as driving data of the deforestation area. The area estimates are calculated based on observations from satellite data (e.g., Landsat) between August and July (e.g., August 2019–July 2020). Moreover, PRODES/INPE only track deforestation within their old-growth forest mask. The BLUE model uses as the Global Land Use Harmonization database (LUH2) to estimate the area impacted by land use changes, which rely on changes in agricultural areas to model the deforested area within old-growth and secondary forests in a calendar year (January–December). The GFED data used here is based on burned areas estimates associated with deforestation and degradation in tropical forests estimated from satellite data (MCD64 A1 product<sup>46</sup>) in a calendar year (January–December). Therefore, the different map periods in addition to the different methods to calculate the forest area loss, as well as the processes included are likely the reasons for the differences between the INPE estimates and the two other models based on global products.

In old-growth forests, the simulated sink by the TRENDY-v11 DGVMs for the Brazilian Amazon was  $-170$  ( $\pm 144$ )  $Tg\ C\ yr^{-1}$  between 2010 and 2020. This is about 51% of the old-growth sink simulated for the whole Amazon in this study ( $-333 \pm 195\ Tg\ C\ yr^{-1}$ ). Most of the simulated old-growth forests sink is concentrated in the central-western part of the Brazilian Amazon



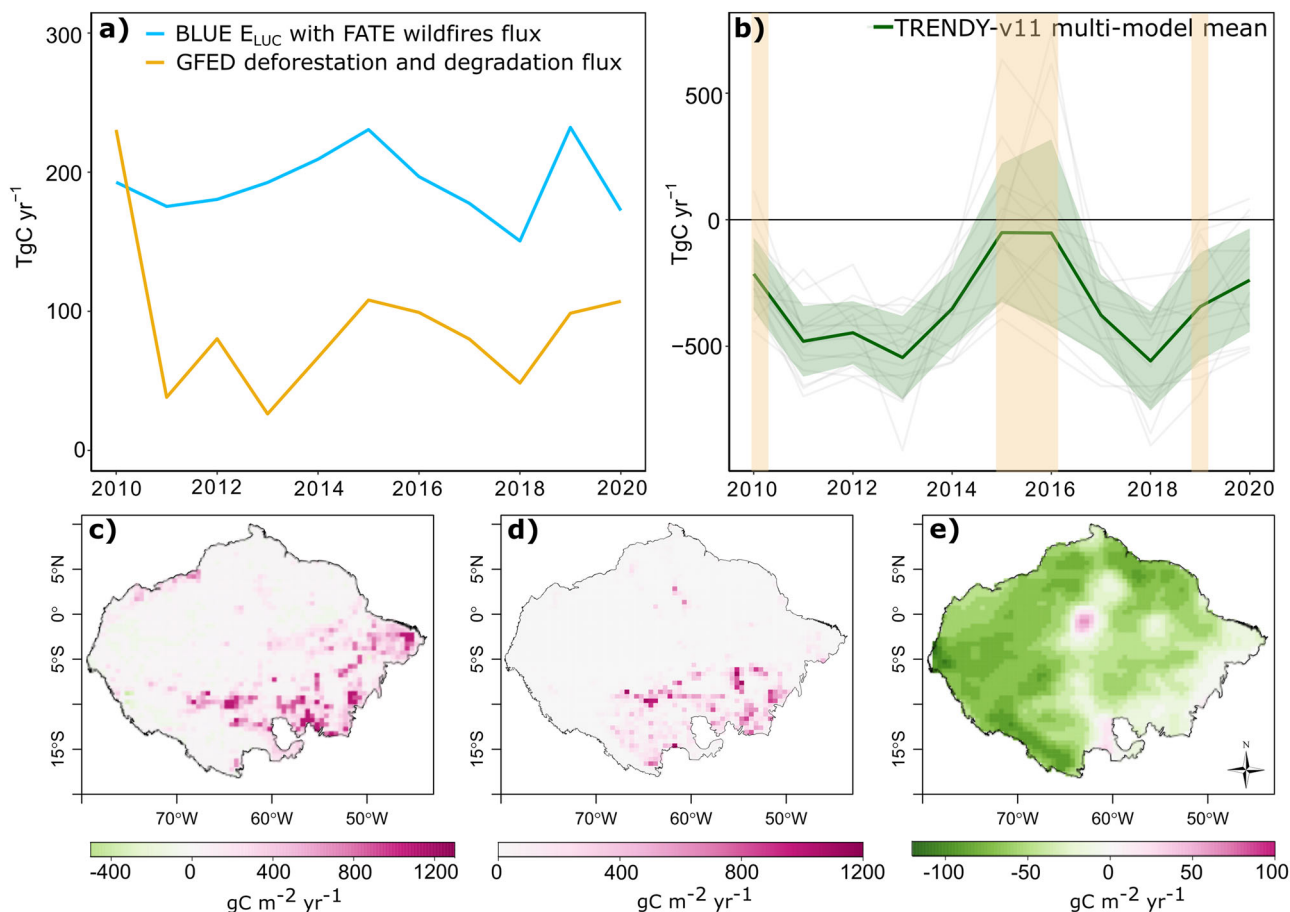


**Fig. 2 Attribution of the land carbon fluxes in the biogeographical Amazon over 2010–2020 from bottom-up and hybrid model combinations.** **a** Annual net disturbance fluxes from BLUE land use and land cover changes (BLUE  $E_{LUC}$ ) with FATE forest degradation fires, and GFED deforestation and degradation fires. **b** Annual old-growth forest sink from TRENDY-v11 S2 simulations; shaded green area represents 1 SD of the multi-model average and shaded orange area represents the ENSO years, which cause strong drought events and consequent water stress in the Amazon forests, and therefore a transition from sink to source in the old-growth forests ( $R = -0.6$ ,  $p = 0.051$ ; see Supplementary Fig. 2c for a correlation between the old-growth sink annual variation and a drought index). **c** Mean annual land use and land cover flux from BLUE with wildfire flux from FATE ( $\text{gC m}^{-2} \text{yr}^{-1}$ ), negative values in this map show a sink from land use abandonment, secondary forest regrowth and/or regrowth after harvest. **d** Mean annual deforestation and degradation fires from GFED ( $\text{gC m}^{-2} \text{yr}^{-1}$ ). **e** Mean annual old-growth forest sink from TRENDY-v11 ( $\text{gC m}^{-2} \text{yr}^{-1}$ ). The spatial uncertainty from the TRENDY-v11 old-growth sink is shown in Supplementary Fig. 10. Positive values (in pink) indicate sources to the atmosphere and negative values (in green) indicate sinks.

(Fig. 3d), where most of the old-growth forests are located. Likewise, as was explained in the Biogeographical Amazon section, the strong pink pattern in the old-growth forest sink (Fig. 3d) is driven by lower annual precipitation during the 2015/2016 ENSO (Supplementary Fig. 3) and the simulated response from DGVMs to this lower precipitation in the decadal mean flux (Supplementary Fig. 4).

#### Net land carbon flux in the whole biogeographical Amazon.

Over the whole biogeographical Amazon, results of the net land carbon flux estimate from the bottom-up, hybrid and data assimilation (e.g., CARDAMOM) approaches suggest that the region was a net land carbon sink of  $-152(\pm 192) \text{ Tg C yr}^{-1}$ ,  $-255(\pm 192) \text{ Tg C yr}^{-1}$  and  $-339 \text{ (CI } -2945 \text{ } -2452) \text{ Tg C yr}^{-1}$  between 2010 and 2018, respectively (Fig. 4a and Table 1). The top-down inversion suggests a small net land carbon source of  $+27 (\pm 130) \text{ Tg C yr}^{-1}$  (2010–2018) (Fig. 4a, Table 1). During the drought years of 2010 and 2015/2016, the bottom-up, hybrid, and top-down inversion approaches agree that the whole Amazon was a small net carbon source while CARDAMOM suggests it was carbon neutral. Over 2019 and 2020, the bottom-up, hybrid, and CARDAMOM estimates suggest the whole biogeographical

Amazon to be a net land carbon sink (Table 1). However, large uncertainties remain in all estimates. Spatially, all the models show that the south-eastern Amazon (Fig. 4b, c and Supplementary Figs. 14b, 15a) was a carbon source to the atmosphere driven by land use and land cover changes, forest degradation and the effects of intense drought events such as the strong 2015/2016 El Niño.

#### Net land carbon flux in the Brazilian Amazon.

For the Brazilian Amazon, we combined the disturbance flux from the multi-model average (Fig. 3a, black line) with the simulated sink in old-growth forests (Fig. 3b, dark green line) to provide a bottom-up estimate of the net land carbon flux alongside the top-down inversion (see Methods for detailed information). The results from the bottom-up approach suggest that the Brazilian Amazon had a small net land carbon sink of  $-59 (\pm 160) \text{ Tg C yr}^{-1}$  over the 2010–2018 period (Fig. 5a and Table 1). Conversely, the top-down inversion suggests the same region as a small net carbon source of  $+36 (\pm 125) \text{ Tg C yr}^{-1}$  over 2010–2018. However, given the large uncertainties in both approaches, their mean estimate over 2010–2018 is not statistically significantly different (Welch's  $t$  test  $p = 0.13$ ; Supplementary Fig. 11). Both approaches agree that the

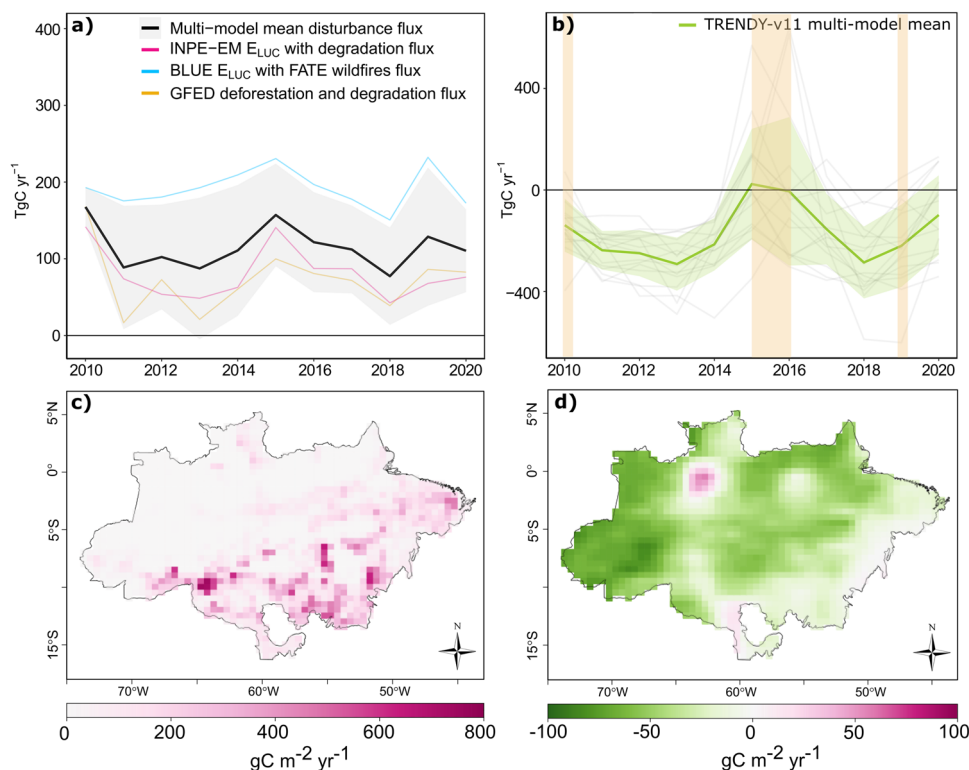


**Fig. 3 Attribution of the land carbon fluxes in the Brazilian Amazon over 2010-2020 from bottom-up models.** **a** Annual net disturbance fluxes from the disturbance multi-model average (see Tables 2-3 in Methods section); shaded grey area represents the 1SD of the multi-model average; individual uncertainty is not available for each model. **b** Annual old-growth land sink from TRENDY-v11 S2 simulations; shaded green area represents the 1SD of the TRENDY-v11 DGVMs mean and shaded orange areas represent the ENSO years, which cause stronger drought events in the Amazon and consequent water stress and therefore a reduction in the old-growth sink ( $R = -0.88$ ,  $p < 0.001$ ; see Supplementary Figure 2b for a correlation between the old-growth sink annual variation and a drought index). **c** Multi-model mean annual disturbance flux ( $\text{gC m}^{-2} \text{yr}^{-1}$ ). **d** Multi-model mean annual old-growth land sink from TRENDY-v11 S2 simulation ( $\text{gC m}^{-2} \text{yr}^{-1}$ ). The spatial uncertainty of (c) and (d) can be found in Supplementary Fig. 7. Positive values (pink) indicate a net carbon source to the atmosphere and negative values (green) indicate a net sink.

Brazilian Amazon was a net carbon source during the drought events of 2010 and 2015/2016. Spatially, the bottom-up approach (Fig. 5b) and the top-down inversion (Supplementary Fig. 15a) agree that the south-eastern Brazilian Amazon was a net carbon source over the period of 2010-2020. Estimates from the bottom-up approach show that the Brazilian Amazon transitioned from a net land carbon sink of  $-91 (\pm 186) \text{ Tg C yr}^{-1}$  in 2019 to a small net land carbon source in 2020 of  $+12 (\pm 165) \text{ Tg C yr}^{-1}$ , driven by a decrease in the simulated old-growth forest sink by TRENDY-v11 DGVMs and in addition to large disturbance fluxes (Table 1).

There are some differences between the bottom-up and top-down inversion estimates of the net land carbon flux. The most evident difference is the opposing sign of the net land carbon flux in 2012 and 2018 between top-down and bottom-up/hybrid models. This difference is present in all model estimates over both the whole Amazon (Fig. 3a) and Brazilian Amazon (Fig. 5a). The top-down inversion suggests a net carbon source in 2018, which is hypothesized to be related to reduced carbon uptake in the south-eastern Amazon<sup>32</sup>. Our bottom-up attribution shows a net lower disturbance flux in 2018 compared to 2015-2017 and a larger sink from old-growth forests (i.e., uptake), thus suggesting a net land carbon sink in 2018. We hypothesize that the large flux from the top-down inversion can be partly attributed to the difference in the spatial resolution of the datasets. For instance, the atmospheric inversion has a spatial resolution of  $5.6^\circ$ , therefore it could be potentially accounting for surrounding fluxes within these large grid-cells, such as fluxes from savanna

fires and additional fluxes coming from fossil fuel emissions; these large fluxes are mostly from locations in the south and east Amazon (see 2012 and 2018 maps in Supplementary Figure 12). The models used to estimate the net land carbon flux using the bottom-up approach have a spatial resolution that ranges from 30 m to  $1^\circ$  ( $\sim 100 \text{ km}$ ) and are then expected to better constrain regional/local fluxes than the coarse spatial resolution of the top-down inversion. However, the bottom-up approach used to estimate the net land carbon flux in this study needs to be considered as a conservative estimate (i.e., potentially under-estimating) the extent and magnitude of the disturbance flux due to difficulties in mapping understory fires as well as by not including additional fluxes associated with edge effects, for example, and limitations to represent the long-term impact of tree mortality on the carbon sink of old-growth forests from DGVMs. Thus, the top-down inversion could be capturing fluxes that are missing in the bottom-up approach, which could also contribute to explain the differences in specific years as well as in the magnitude and sign of the net land carbon fluxes.

## Discussion

Our total net disturbance flux estimates by bottom-up models suggests an average offset of about 68% and between 27%-58% of the old-growth forest carbon sink of Brazilian Amazon and biogeographical Amazon, respectively, between 2010 and 2020. Net forest disturbance emissions are large in 2010 and 2015, which is likely related to increases in wildfires in the Amazon as an

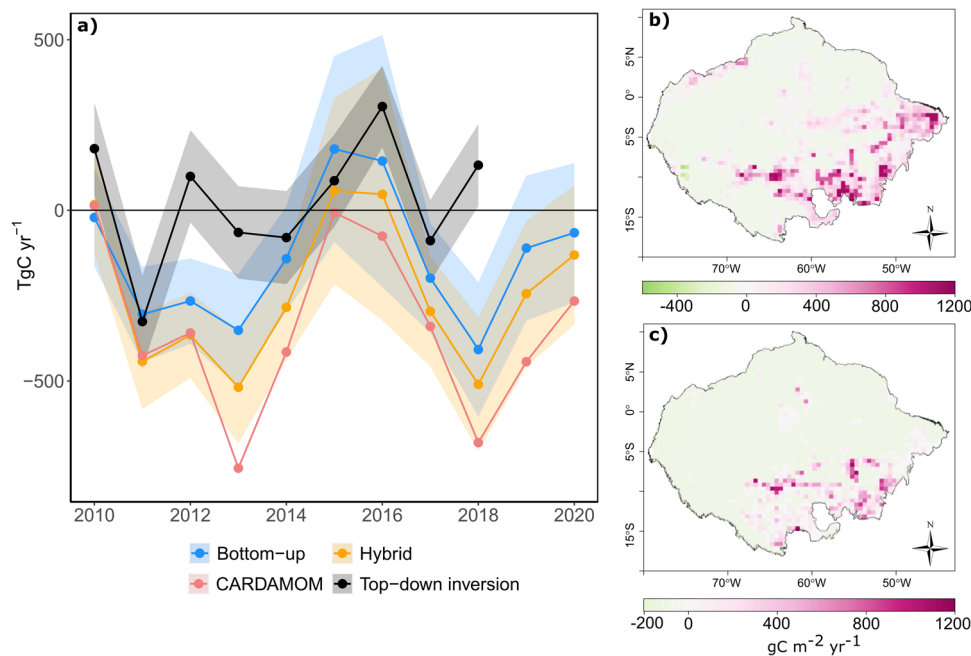


**Fig. 4** The net land carbon fluxes in the biogeographical Amazon. **a** Annual net land carbon fluxes from the two bottom-up approaches using the anthropogenic disturbance estimates from BLUE land use and land use changes and forestry added to FATE wildfire flux estimate (Bottom-up) and GFED deforestation and degradation fluxes (Hybrid), both added to the TRENDY-v11 intact land sink to yield the net land carbon flux; the net land carbon flux from CARDAMOM model and top-down atmospheric inversion. **b** Spatiotemporal average of the net land carbon flux from the bottom-up approach (2010–2020) using the disturbances from BLUE land use and land cover changes emissions with FATE wildfire flux and TRENDY-v11 intact sink ( $\text{gC m}^{-2} \text{yr}^{-1}$ ). **c** Spatiotemporal average of the net land carbon flux from the Hybrid approach (2010–2020) using the GFED deforestation and degradation fluxes and TRENDY-v11 intact sink ( $\text{gC m}^{-2} \text{yr}^{-1}$ ). The CARDAMOM uncertainty and spatial net average flux (2010–2020) can be found in Supplementary Fig. 14. The top-down spatial average net flux and its uncertainty can be found in Supplementary Fig. 15. Spatial uncertainty associated with the TRENDY-v11 old-growth forest sink over 2010–2020 can be found in Supplementary Fig. 10, both BLUE and GFED do not provide regional uncertainties. Positive values are source to the atmosphere and negative sink.

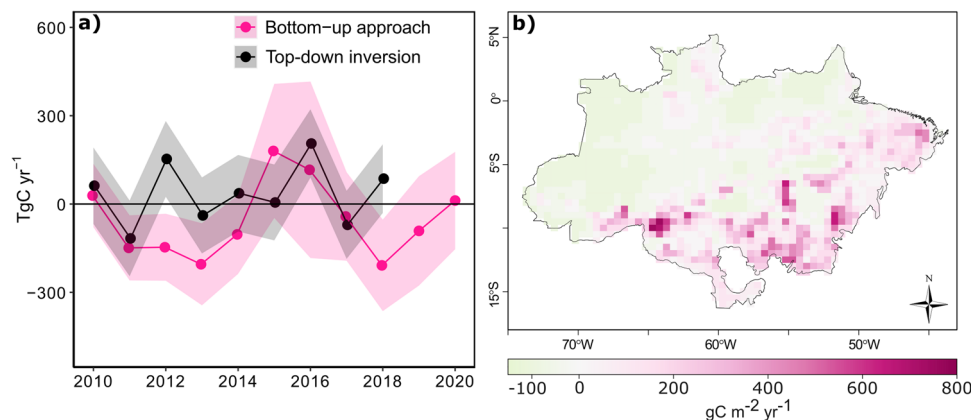


**Fig. 5** The net land carbon fluxes in the Brazilian Amazon. **a** Annual net land carbon fluxes from the bottom-up approach using the combination of the multi-model mean net anthropogenic disturbance flux and TRENDY-v11 old-growth sink and top-down atmospheric inversion; shaded area represents the propagated error of both approaches (see methods). **b** Spatial explicit bottom-up net land carbon flux over 2010–2020 ( $\text{gC m}^{-2} \text{yr}^{-1}$ ). The spatial uncertainty over 2010–2020 can be found in Supplementary Figure 13. Positive values are sources of the atmosphere and negative values are sinks.

outcome of anthropogenic activities in combination with intense drought<sup>17</sup>. The increase in the net disturbance emissions after 2018 is associated with an escalation in fire activity related to recent increases in deforestation rates<sup>47,48</sup>. This recent change in deforestation pattern, mostly in the Brazilian Amazon, is in response to a combination of changes in the Brazilian Forest Code in 2012, recent weakening of the Ministry of the Environment's deforestation enforcement actions, and laws that may facilitate the regularization of illegally grabbed public lands<sup>49,50</sup>. If

this current pattern of deforestation remains, it will likely contribute to further offsetting the old-growth forest carbon sink.

However, high uncertainties remain on the magnitude of the net disturbance fluxes, as well as the old-growth forest sink and its impacts on the Amazonian carbon balance. Previous studies have shown that the bookkeeping models used in earlier Global Carbon Budget assessments were not able to capture the magnitude and trend of land use changes for the Amazon in recent years due to deficiencies in the input data<sup>36,51</sup>. Major improvements were

achieved by incorporating further satellite Earth Observation (EO) data for Brazil into the land use change data that are used as input in the BLUE model simulations for the Global Carbon Budget 2022<sup>39</sup>, which we employ here.

We also used estimates of a fire bookkeeping model (FATE) that quantifies the long-term net carbon fluxes of burned forests in the Amazon based on inventory data from burned forests and upscales them to the Brazilian Amazon using burned area maps. Yet, this is a conservative estimate (i.e., likely an underestimate) linked to limitations of mapping the extent of burned forests in the Amazon. Uncertainties are caused by 1) difficulties in mapping low intensity understory fires; 2) limited temporal availability of Landsat images used in FATE (i.e., the satellite passes over the same region twice per month, but since the Amazon has high cloud cover it limits the number of images available for classification)<sup>52</sup>. With the increasing availability of medium to high spatial resolution satellite images, such as the Sentinels from the Copernicus program, as well as higher temporal availability by integrating a range of images of different satellites, this limitation might be overcome in the future. Further work is needed to expand the wildfire emission estimates to the whole biogeographical Amazon using a set of aboveground biomass data and burned area products. This would allow a sensitivity analysis using different input data to better quantify the uncertainties related to the long-term effect of forest degradation through fire on the carbon balance.

Edge effects caused by fragmentation can induce indirect carbon losses, which were estimated to have caused gross emissions of 63 Tg C yr<sup>-1</sup> for 2001–2015<sup>22</sup>. This individual flux is unquantified in this research and should be included in future land carbon flux assessments. However, we do partially account for edge effects due to overlap of wildfires in forest edge areas, which is estimated to be around 25% of the total burned forest area<sup>19</sup>. The inclusion of additional edge effects would be possible by standardizing the same input dataset for the bottom-up models, such that we could overlay the edge and burned forest areas and separate each flux correctly. Moreover, currently, there are still knowledge gaps on forest edge dynamics to produce estimates of its net carbon flux combined with wildfires on the Amazon carbon balance<sup>19</sup>. For example, the few models that consider edge effects only include gross carbon fluxes and not the potential partial recovery. Therefore, the total disturbance flux estimate from this work can be considered conservative.

Additionally, large uncertainties remain about the contemporary trends and magnitude of the old-growth Amazon forest sink. Observations show a weakening of the Amazon Forest sink<sup>9</sup>. Yet, the TRENDY-v11 multi-model mean shows no significant trend in the old-growth forest sink in the last 30 years<sup>53</sup> (Supplementary Figure 16). The large flux and no significant decline in the old-growth forest sink simulated by TRENDY-v11 DGVMs is likely due to the lack of detailed processes related to drought-induced mortality and plant hydraulics, such as potential legacy effects from droughts that are not well represented<sup>35</sup>. It has been estimated that approximately 41% of the whole Amazon forest has been impacted by strong drought events between 2001–2018<sup>19</sup> and one weak, and two moderate to strong drought events happened during our study period (Supplementary Fig. 2). Thus, we hypothesize that despite simulating reductions in plant productivity during drought, current estimates from DGVMs are likely underestimating the long-term impact of contemporary drought-induced mortality over Amazon forests. Current studies investigating the fate of the Amazon under climate change using seven Earth System Models from Phase 6 of Coupled Model Intercomparison Project, CMIP6, indicate localized future reductions in vegetation carbon across Amazon by 2100<sup>54–56</sup>. The inclusion of long-term drought-induced tree mortality in current

model developments is a priority, and will likely improve Earth System model representation of carbon stocks and fluxes<sup>57</sup>, thus providing a better quantification of the future evolution of the Amazon in response to climate change.

Given the large uncertainties from the models used in this research, as well as the remaining knowledge gaps on the impacts of forest disturbances on the carbon balance of Amazon, we have insufficient data to confirm whether the whole Amazon was a carbon source, a carbon sink or carbon neutral over the contemporary period according to the bottom-up methods (2010–2020) and the top-down inversion (2010–2018). Our study does however provide further evidence from a range of bottom-up models, as well as top-down inversion that the south-east Amazon was a net land carbon source over the analyzed time period. This result is also corroborated by airborne measurements<sup>32</sup>. This area of the Amazon has warmed and dried in recent years, particularly during the dry seasons, and it is subject to higher rates of deforestation and fire activity compared to the western Amazon, thus it has increased carbon losses and emissions with compromised forest resilience<sup>58–60</sup>.

Further studies are needed to reconcile the bottom-up and top-down estimates of the net land carbon balance of the Amazon region used in this study. Key areas for future developments are (1) the exploration of how to separate the influence of fluxes from areas surrounding the Amazon due to atmospheric transport of greenhouse gases on the net land carbon fluxes from the top-down inversion; (2) a better representation of drought-induced tree mortality in DGVMs; (3) improved estimates of the impact of forest degradation, including the edge-effect, as well as deforestation on the net land carbon fluxes; (4) improved uncertainty estimations of input data used by bottom-up and top-down models. This could provide a better constraint of local/regional net land fluxes and possibly reconcile estimates based on medium-to-high spatial resolution models, such as the bottom-up approach used in this research. Finally, it is very important to expand and maintain long-term field-inventory measurements, in both old-growth and degraded forests, as well as atmospheric greenhouse gas measurements for model parametrization and quantification of uncertainties.

## Conclusion

We provide a state-of-the-art assessment of net land carbon fluxes, the old-growth forest sink, and the anthropogenic forest disturbance for the Amazon using bottom-up and top-down approaches, over 2010–2020. Our analysis shows that we still do not have sufficient data to reconcile bottom-up and top-down estimates of the net carbon balance of Amazon. Spatially, all the model combinations and the top-down inversion suggest that the south-eastern part of the Amazon was a net source of carbon over the analyzed period due to deforestation, the impacts of wildfires, and climate trends. This finding agrees with previous studies based on atmospheric greenhouse gases measurements<sup>32</sup>. Consequently, the south-eastern Amazon acting as net carbon source now may have long-term effects on the Amazon carbon balance, compromising the mitigation potential of the Amazon Forest and the resilience of this ecosystem in a changing climate.

## Methods

The key terms in the contemporary net land carbon balance of the Amazon are: (i) human disturbance fluxes (i.e., anthropogenic flux) due to land use and land cover changes and degradation, and (ii) the old-growth forests sink (i.e., natural sink). In this section, we first present the models used to attribute and estimate the net disturbance fluxes and the net old-growth forest sink over the Brazilian Amazon and Biogeographical Amazon. We then



describe the approach used to estimate the net land carbon fluxes with the atmospheric inversion and the combination of the source and sink components from various models.

**Disturbance fluxes attribution.** We used a set of models to estimate net emissions from different forest disturbance components, such as deforestation, land use and land cover change, and degradation. Note, these disturbance fluxes are reported from different products and can overlap in terms of processes which are defined in Table 2. In this study, we combine different products such that we avoid double-accounting fluxes from the same process. Table 2 includes the main models used to attribute the disturbance fluxes. Further details of each model are given below.

**INPE emission model (INPE-EM).** The INPE-EM is a regional, spatially explicit bookkeeping model to estimate carbon emissions from deforestation based on the bookkeeping model developed by Houghton et al.<sup>61,62</sup> and adapted to the Brazilian Amazon<sup>26</sup>. INPE-EM accounts for the spatial distribution of biomass stocks and observed deforestation by considering the intra-regional diversity of land use changes practices<sup>26</sup>.

In this study, we use INPE-EM to provide consolidated estimates of deforestation without degradation (these are accounted for separately) from 2010 to 2020 (available at <http://inpe-em.ccst.inpe.br>) to estimate the annual net deforestation flux for the Brazilian Amazon. The net deforestation estimates from INPE-EM include emissions from clear-cutting of old-growth forests based on official Brazilian deforestation data, called PRODES (Deforestation Monitoring Project in the Legal Amazon by Satellite). It also accounts for the dynamics of regrowth and deforestation of secondary forests and legacy emissions from deforestation in previous years. INPE-EM also provides separate estimates of degradation, which include the trajectories and dynamics of forest degradation (e.g., fire and logging emissions and recovery). The disturbance estimates from INPE-EM used in this study includes the net integrated estimate using deforestation, degradation, and secondary forest fluxes. The degradation input data for INPE-EM is from the satellite-based Brazilian degradation monitoring system<sup>30</sup>; we used the DEGRAD product up to 2016 and the DETER-B product thereafter<sup>30</sup>. The dynamics of secondary forests implemented in the INPE-EM is based on the land use and land cover maps from the TerraClass product<sup>63</sup> and the cycles of regrowth and clear-cut of secondary forests from ref. <sup>64</sup>. Details on default parameters used by INPE-EM for each component can be found in Supplementary Table 1. Uncertainty estimates are not available for this model because of the difficulties to estimate uncertainty of each input dataset and parameter.

To produce the maps of net fluxes of deforestation and degradation, we used the gridded data from INPE-EM. The original resolution of the INPE-EM spatial output is 5-km and contains the aggregated emission of each grid-cell and comes in a shapefile format. This data was then converted to raster format and re-gridded to 0.5° spatial resolution by aggregating the grid-cells with the sum of fluxes.

**Bookkeeping of Land Use Emissions (BLUE).** The Bookkeeping of Land Use Emissions (BLUE)<sup>25</sup> is a spatially explicit global model that tracks carbon emissions and removals due to historical changes and interactions of LULCC in each grid cell. BLUE follows the bookkeeping approach developed by Houghton et al.<sup>62,65</sup>. BLUE considers the conversion of natural vegetation to agriculture (cropland and pasture) and abandonment<sup>66,67</sup>. It also includes gross transitions at the sub-grid scale ('shifting cultivation'), transitions between cropland

and pasture, and wood harvesting, and accounts for legacy fluxes associated with LULCC over time. The model distinguishes 11 natural plant functional types (PFTs). Average equilibrium biomass densities for the 11 PFTs and cropland and pasture are based on observation-based literature, as are the dynamics of carbon gains or losses, represented via PFT and process-specific response curves, following land-use change and wood harvesting (for the Tropical PFTs see Supplementary Table 2)<sup>25</sup>. Here we use the BLUE simulations that were performed for GCB 2022<sup>39</sup>.

The land use forcing data used for BLUE in GCB 2022 and thus in our study is the gridded LUH2 data set<sup>66,67</sup> (GCB 2022 version), which provides historical sub-grid-scale transitions between land-use and land-cover categories, such as primary and secondary natural land, cropland, pasture, rangeland, and urban land<sup>66,67</sup>. LUH2 incorporates multiple datasets at different spatial and temporal scales to produce a global gridded land use dataset. For example, it uses inputs from the History Database of the Global Environment (HYDE 3.3)<sup>68</sup> for cropland and grazing areas, which are derived from FAO (Food Agriculture Organization) national statistical data (and sub-national where available) and spatially allocated based on the ESA Climate Change Initiative (ESA CCI) land cover annual maps<sup>66,67</sup>. Therefore, the LUH2 natural vegetation cover is not constrained directly by observations, such as remote sensing data. Recently, there has been a major update in the LUH2/HYDE 3.3 (GCB 2021 version) in cropland and pasture areas for Brazil derived from Food and Agriculture Organization (FAO) national statistics due to double-cropping issues<sup>69</sup>, and the adoption of multi-year ESA CCI land cover maps. This update improved the spatial allocation of land use changes within Brazil, but it still underestimated the fluxes estimates when based directly from remote sensing products such as the MapBiomass LULCC maps<sup>36</sup>. Furthermore, there is latency in FAO statistics, and annual data until 2017 was used in HYDE3.3. To extrapolate to the end of 2021, a trend from the last five years of data (2012-17) is typically applied, which does not capture the recent upturn in deforestation for Brazil<sup>13</sup>. To better represent and improve the magnitude of LULCC in Brazil and consequently in the Amazon, the cropland and grazing areas of LUH2/HYDE3.3 (GCB 2022 version) dataset for the years 1700-2021 used by BLUE<sup>39</sup> was based on the areas derived from the remote sensing classification from MapBiomass (collection 6) maps at state level for the contemporary period (1985 until year 2020), and then spatially allocated by the HYDE 3.3 algorithm. Due to the challenges of estimating uncertainties of input parameters from the BLUE model, there is currently no regional uncertainty estimate available.

In this study, we provide estimates of the net land use and land cover change emissions ( $E_{LUC}$ ) for both study regions (Brazilian Amazon and Biogeographical Amazon) from the global BLUE model. To produce the  $E_{LUC}$  maps, BLUE output at 0.25° spatial resolution was converted to raster format and re-gridded to 0.5° of spatial resolution with the aggregated sum of the fluxes.

**FATE forest degradation fire flux estimate.** The fire bookkeeping model (FATE) is a spatiotemporal model to estimate long-term net emissions from Amazon Forest fires. This is a spatially explicit approach based on<sup>21</sup> which has been developed in partnership with the Brazilian Greenhouse Gas Emission and Removal Estimating System (SEEG) project and FATE network. The model is parametrized with a dataset derived from field information of burned plots in the Amazon and includes estimates of combustion emissions, as well as post-fire temporal biomass changes and delayed mortality and recovery<sup>21</sup>. The

**Table 2 Models used to attribute disturbance fluxes for the Brazilian Amazon\* and for the whole Biogeographical Amazon†.**

Model	Disturbance area input	Biomass input	Spatial Resolution	Extent	Emissions uncertainty	Gross or net	Main processes	Model reference
<b>*INPE-EM</b>	Based on remote sensing observation; Deforestation areas from PRODES; Degradation areas from DEGRAD and DETER-B;	Spatial: 4th National Inventory of Greenhouse Gases (Brazil MCTI, 70)	Output 5x5km Input 30mx30m	Brazilian Amazon	NA	Deforestation and degradation gross source and sink flux based on literature response curves (see parameters details in Supplementary Table 1)	Deforestation in old-growth forest only and forest degradation (e.g., forest degradation by fire and logging)	Aguar et al. <sup>32</sup> ; Assis et al. <sup>24</sup>
<b>*BLUE</b>	Based on the Land Use Harmonization 2 (LUH2) dataset. This product uses information on agricultural areas based on the History of the Global Environmental database (HYDE). HYDE is based on in-country FAO statistics and uses the ESA CCI Land Cover maps to scale the in-country areas from FAO to global, spatially explicit estimates. For Brazil it constrains the cropland and grazing areas using MapBiomas c6 areas at the state level. For wood harvest, LUH2 uses FAO/FRA statistics.	Biome level carbon stocks based on literature (Hansis et al. <sup>25</sup> )	0.25°x0.25°	Global	NA	Land use and land use change and forestry gross source and gross sink flux based on carbon densities and response curves from literature (see parameters details in Supplementary Table 2)	Clearing of natural vegetation, including forests, for agricultural expansion (including in shifting cultivation); degradation through logging or use of natural vegetation for rangelands, regrowth of natural vegetation after agricultural abandonment and logging.	Hansis et al. <sup>25</sup>
<b>*GFED</b>	Based on remote sensing observation; Burned area is derived from the Moderate Resolution Imaging Spectroradiometer (MODIS).	Biome level; Modelled by CASA	0.25°x0.25°	Global	1σ 50% (Global)	Net immediate fire fluxes	Deforestation and degradation fires. GFED considers burned forests are carbon neutral in the long-term. So, GFED presents only immediate emissions and does not account for emissions	van der Werf et al. <sup>40</sup>

**Table 2 (continued)**

Model	Disturbance area input	Biomass input	Spatial Resolution	Extent	Emissions uncertainty	Gross or net	Main processes	Model reference
* <sup>i</sup> FATE	Based on remote sensing observation; Burned area from MapBiomass fire collection 1 (beta version)	Spatial; Carbon stocks from 4th National Inventory of Greenhouse Gases (Brazil MCTI, <sup>70</sup> )	30mx30m	Brazilian Amazon	NA	Net flux based on field-inventory relationship and scaled-up with remote sensing data (Silva et al, <sup>21</sup> )	from late tree mortality due fire occurrence. Long-term net carbon balance of degradation fires in burned forests not deforested up to 2020. FATE accounts for late tree mortality fluxes due fire occurrence.	Silva et al. <sup>21</sup>

model is scaled-up to the Brazilian Amazon using the time-series of burned area (MapBiomass fire collection 1)<sup>52</sup> and the biomass map derived from the 4th National Communication of the National Inventory of greenhouse gases (MCTIC,2020).

This burned area product is based on a time-series of Landsat mosaics for the entire Brazil with spatial resolution of 30mx30m over the period 1985-2020. To classify the burned pixels, MapBiomass fire uses a deep learning algorithm (Deep Neural Network) within the Google Earth Engine platform. The methodology also takes advantage of ancillary data, such as the burned area product MC64A1 and the fire hotspot data from INPE to train the algorithm. The reported average accuracy of burned areas from MapBiomass fire was 89.35%<sup>52</sup>. However, it presents a conservative estimate (i.e., an underestimate) due to the limitations associated with the temporal availability of Landsat images, mainly in areas with high cloud coverage, such as the Amazon and the difficulty to map low-intensity understory fires<sup>52</sup>.

To estimate only the emissions from degraded forests by fire, the burned area product was overlaid with the deforestation data and LULCC maps from MapBiomass to exclude the pixels that were deforested (e.g., deforestation fires) and fires outside forest pixels. The biomass product from the 4th National Inventory of Greenhouse Gases<sup>70</sup> was used to estimate the biomass stocks and necromass. The mortality parameters were based on a previous study<sup>21</sup> and additional permanent plots with measurements before and after fires, and the combustion loss and decomposition parameters were derived from literature. Formal uncertainty is not provided due to difficulties in propagating the uncertainty of the input data. The spatial output is available at a 30mx30m spatial resolution with the net CO<sub>2</sub> flux over 1985-2020. To convert to carbon, we multiplied the values by the conversion factor CO<sub>2</sub>-C of 12/44. We then summed the values within the Brazilian Amazon limits to produce the total annual data. To produce the spatial maps of net CO<sub>2</sub> flux of burned forests from forest degradation by fire in the Brazilian Amazon, we aggregated it to 0.5° spatial resolution using the sum of the grid cells to facilitate the comparison with the global models at a coarse spatial resolution. In this study, we add the FATE forest degradation flux from the Brazilian Amazon to E<sub>LUC</sub> from BLUE (which lacks degradation from fires) to provide an integrated estimate of the total disturbance from land use and land cover changes emissions and degradation.

**Global Fire Emissions Database (GFED).** As an additional estimate of the disturbance emissions from deforestation and degradation for both the Brazilian Amazon and the whole Biogeographical Amazon, we used the Global Fire Emissions Database (GFED4.1s). The GFED is a modelling system based on the Carnegie-Ames-Stanford Approach (CASA) biogeochemical model and has a spatial resolution of 0.25° x 0.25°<sup>40</sup>. The burned area input of GFED is derived from MODIS (MCD64A1 product)<sup>46</sup>, which provide daily burned area at 500 m spatial resolution and then GFED aggregates to a 0.25° grid. Formal uncertainty is not provided by GFED due to difficulties in assessing uncertainty of various layers used in the modelling. However, the best-guess global uncertainty provided could be 1σ 50%<sup>40</sup>. In our analysis we extracted and aggregated the GFED annual emissions associated with tropical forest fires, which include burned biomass due to both deforestation and degradation processes, within both the Brazilian Amazon and the whole Biogeographical Amazon limits. Then, the spatial GFED maps were aggregated to 0.5° spatial resolution using the sum of the grid-cell fluxes.

**Old-growth Forest carbon sink estimates.** The old-growth forest sink was estimated from a multi-model mean of 16 DGVMs from the Trends in the land carbon cycle project (TRENDY-v11), using the simulations performed for GCB 2022<sup>39</sup>. Each DGVM performed factorial simulations for TRENDY-v11 to attribute the carbon exchange to individual environmental drivers. To estimate the old-growth forest sink we used TRENDY-v11 simulation 2 (S2) which uses time varying atmospheric CO<sub>2</sub> concentrations, nitrogen deposition, and climate with a time-invariant pre-industrial (year 1700) land cover distribution. This approach is used by the Global Carbon Budget assessments to calculate the natural terrestrial sink. More details about the DGVM processes relevant for the intact sink can be found in Supplementary Table 3. S2 does not account for LULCC dynamics, and thus includes the impact of environmental changes on land that in reality has been modified by humans. This leads to a large CO<sub>2</sub> induced carbon sink in forests that existed in 1700, but do not exist anymore today. Previous work estimated this additional carbon flux to be ~100 Tg C yr<sup>-1</sup> for Brazil over 2000–2020<sup>71</sup>. To mask out the proportion of the old-growth sink within disturbed grid-cells and account only for the sink from old-growth forests, we used a mask from INPE based on the Brazilian Amazon official annual accumulated deforestation data available since 1988 and for degradation data since 2007 (Supplementary Figure 5). To maintain consistency in the old-growth forest mask, we used only the official data provided from INPE since it has a better manual control of its forest mask over time compared to other remote sensing-based products that rely on automatic classification and just account for degradation in primary forest pixels. However, this data is available only for Brazil and the degradation estimates start in 2007; consequently, it constitutes a conservative estimate of the old-growth forest fraction. Therefore, the old-growth sink estimates obtained with this mask could potentially still overestimate part of the natural sink in the non-Brazilian Amazon countries (i.e., western and north region). The application of this mask reduced the whole Amazon natural sink simulated by TRENDY-V11 models from -362 (±220 1 SD) Tg C yr<sup>-1</sup> to -333 (±195) Tg C yr<sup>-1</sup> over 2010–2020 (Supplementary Figure 8). We applied this mask to each DGVM from TRENDY-V11. Then the annual old-growth sink was extracted for each model within the limits of both the Biogeographical Amazon shapefile and the Brazilian Amazon biome. Finally, we calculated the multi-model mean and standard deviation statistics. To evaluate the correlation between the annual variation of the old-growth forest sink and the drought effects from ENSO years, we used as a drought metric the Annual Maximum Cumulative Water Deficit<sup>43</sup> (MCWD) based on the precipitation data from CRUJRA2.4<sup>72–74</sup>. The MCWD is an indicator of meteorologically induced water stress in forests. We then extracted the average annual MCWD within the Brazilian Amazon and Biogeographical Amazon domains and performed a correlation analysis (Pearson's correlation test) between the annual old-growth forest sink and the MCWD. In order to assess the old-growth sink simulated by the DGVMs, we compared it against RAINFOR inventory-based estimates<sup>8,9,44</sup> for the common period (2010–2015) by using a Welch's *t*-test to test whether the averages over the same period were significantly different. Additionally, we did a similar test comparing the aboveground carbon changes (AGC) in old-growth forests based on L-VOD<sup>12</sup> and the AGC changes based on the TRENDY-v11 multi-model mean between 2011 and 2019. We used the annual biomass data from each model of TRENDY-v11 to calculate the change between the years and compare to AGC based on L-VOD. Since the biomass variable from TRENDY-v11 accounts also for belowground biomass, we assumed that 20% of this biomass is belowground based on previous studies<sup>75</sup> and applied a factor of 0.8 to each grid cell to

extract the aboveground stock. Finally, we performed a Welch's *t*-test to test whether the averages over the same period were significantly different.

**Net land flux approaches.** To quantify the net carbon exchange flux between land and atmosphere we used the chemical transport model TOMCAT<sup>76</sup> and its inverse model, INVICAT<sup>77</sup>. The data was produced using a variational (4D-var) inverse model to optimize monthly non-fossil fuel land and ocean carbon fluxes through assimilation of in situ flask data from the Global Monitoring Laboratory (GML) of the National Oceanic and Atmospheric Administration (NOAA)<sup>78</sup>. A new addition to this model was the use of independent in situ lower-troposphere observations by aircraft-borne flask of greenhouse gases (CO<sub>2</sub>) made within the Amazon basin since 2010<sup>48</sup>, thus providing a better-constrained regional estimate. The a priori inversion input was based on the Carnegie-Ames-Stanford model (CASA) for land fluxes. A climatology was used as a prior for the CASA fluxes, so all posterior variation was provided by the atmospheric observation data and varying meteorology. In addition to the CASA land fluxes as prior, TOMCAT inputs include fossil fuel data from the Carbon Dioxide Information Analysis Center (CDIAC) and ocean flux was a combination of gridded estimates<sup>79,80</sup>, as in previous TOMCAT inversions<sup>78</sup> scaled to the Global Carbon Project (GCP) values. Prior emissions are given grid cell uncertainties of 308% of the prior flux value. Also, for the assimilated observation data from both surface monitoring sites and the vertical profile sites<sup>81</sup> uncorrelated random errors of 1 ppm were attributed to each observation. The TOMCAT output is available as monthly estimates between 2010 and 2018 with a 5.6° x 5.6° spatial resolution<sup>38</sup>. In our analysis we calculated the annual mean of each grid cell for each year and then the total fluxes within the Brazilian Amazon and Biogeographical Amazon limits.

To calculate a 'bottom-up' approach of the net carbon flux, we first combined the net source (deforestation + degradation) and net natural sink in old-growth forests from TRENDY-v11 S2 simulation, which is similar to the Global Carbon Budget annual assessments methodology. As the net source term (+) for the Brazilian Amazon, we used a multi-model average of the regional bookkeeping model (INPE-EM with degradation), the global bookkeeping model (BLUE) with the net forest degradation flux from FATE added, as well as deforestation and degradation fire emissions from GFED (Table 3). For the Biogeographical Amazon, due to data availability limitations, the disturbance term was based separately on bottom-up and hybrid approaches (see Table 3). A summary of the main input and processes within each of the disturbance models can be found in Table 2. The old-growth forest sink term (-) was calculated using the annual multi-model average from TRENDY-v11 DGVMs over 2010–2020. To calculate the uncertainty of the net land carbon fluxes from the 'bottom-up' approach, we propagated the uncertainty by using the annual standard deviation of the average disturbance estimate and old-growth forest sink based on DGVMs. Since the bottom-up disturbance models differ in their spatial extent (e.g., Brazilian Amazon and Biogeographical Amazon), we used a different combination for each region (Table 3). Spatial model outputs also differ in their spatial resolution and to avoid further error inclusion from spatial resampling, the annual values for the Brazilian Amazon and Biogeographical Amazon were extracted using each model's original spatial resolution. Then, to produce the net carbon flux maps we spatially resampled the bottom-up approaches to a standard spatial resolution of 0.5° x 0.5°.



**Table 3 Components used to calculate the net land carbon flux for the Brazilian Amazon and the whole Biogeographical Amazon.**

Name	Brazilian Amazon	Biogeographical Amazon
Bottom-up	Net disturbance (+): Multi-model average of INPE-EM (deforestation + degradation); BLUE $E_{LUC}$ + FATE net degradation fire flux; GFED (net deforestation and degradation) <sup>b</sup> Net old-growth forest sink (-): TRENDY-v11 Multi-model average <sup>39</sup> The bottom-up net land flux is calculated from the sum of the net disturbance multi-model average and the TRENDY-v11 net old-growth forest sink	Net disturbance (+): BLUE $E_{LUC}$ + FATE net degradation fire flux <sup>a</sup> Net old-growth forest sink (-): TRENDY-v11 Multi-model average <sup>39</sup> The bottom-up net land flux is calculated from the sum of net disturbance flux of BLUE + FATE and TRENDY-v11 net old-growth forest sink
Hybrid	-	Disturbance (+): GFED (net deforestation and degradation) <sup>b</sup> Net old-growth forest sink (-): TRENDY-v11 Multi-model average <sup>39</sup> The hybrid net land flux is calculated from the sum of GFED net fire emissions and TRENDY-v11 net old-growth forest sink
CARDAMOM	-	Net land flux from CARDAMOM model <sup>41,42</sup>
Top-down inversion	Net land flux from TOMCAT atmospheric inversion <sup>38</sup>	Net land flux from TOMCAT atmospheric inversion <sup>38</sup>

Details of each component of the disturbance models are given in Table 2.

<sup>a</sup>Note that the FATE net wildfire flux is available only for the Brazilian Amazon, thus we potentially underestimate this flux for the whole Biogeographical Amazon.

<sup>b</sup>Note that GFED net estimates considers degraded forests by fire as carbon neutral; whereas FATE includes late tree mortality fluxes.

For the whole biogeographical Amazon, we provide an additional estimate of the net land carbon fluxes from the CARbon Data Model fraMework (CARDAMOM)<sup>41,42</sup>. CARDAMOM uses a Bayesian approach within an Adaptive Proposal—Markov Chain Monte Carlo (AP-MCMC)<sup>82</sup> to retrieve parameters, at pixel scale, for the intermediate complexity C-cycle model DALEC<sup>83</sup>. Observational constraints include earth observation datasets and databased information on soil C stocks. Fire is imposed based on the MODIS Burned area product (MCD64A1) while deforestation was imposed based on the Global Forest Watch Forest loss estimates. The atmospheric CO<sub>2</sub> driving dataset was based on the input for the TRENDY-v11 protocol from GCB 2022<sup>39</sup>. The climate driving data was based on Climatic Research Unit gridded Time Series (CRU-TS 4.06)<sup>72</sup> and Climatic Research Unit and Japanese reanalysis data (CRU-JRA v2.4). In this work we used the CARDAMOM version compatible with TRENDY-v11 protocol and the net land carbon fluxes was based on the net biome productivity output from simulation 3 (S3), which accounts for changes in atmospheric CO<sub>2</sub> concentration, climate and land use over time. The output is available as annual estimates over 2000 and 2021 in a global grid of 1° × 1° spatial resolution. Spatial uncertainty estimates were provided by CARDAMOM including explicit propagation of ensemble uncertainty from monthly to annual time scales. The annual net land carbon fluxes and its uncertainty from CARDAMOM were calculated within the limits of the whole biogeographical Amazon region over 2010 and 2020.

### Data availability

The spatial dataset of the main figures are available in a raster format and can be found at <https://doi.org/10.5281/zenodo.10423522>. The annual carbon fluxes from each model used in this research (disturbances, old-growth sink and net flux) for the Brazilian Amazon and whole Biogeographical Amazon are available at <https://doi.org/10.5281/zenodo.8348434>.

### Code availability

The code and tables used to reproduce the main paper graphics of Figs. 2a, b, 3a, b, 4a and 5a are available in Zenodo <https://doi.org/10.5281/zenodo.8348435>. Further editions to combine the layout of graphics and maps were made in a design software (InkScape).

Received: 17 February 2023; Accepted: 5 January 2024;

Published online: 22 January 2024

### References

- Malhi, Y. et al. The regional variation of aboveground live biomass in old-growth Amazonian forests. *Global Change Biol.* **12**, 1107–1138 (2006).
- Gloor, M. et al. The carbon balance of South America: a review of the status, decadal trends and main determinants. *Biogeosciences* **9**, 5407–5430 (2012).
- Feldpausch, T. R. et al. Tree height integrated into pantropical forest biomass estimates. *Biogeosciences* **9**, 3381–3403 (2012).
- Albert, J. S. et al. Human impacts outpace natural processes in the Amazon. *Science* **379**, eabo5003 (2023).
- Lawrence, D. & Vandecar, K. Effects of tropical deforestation on climate and agriculture. *Nat. Clim. Change* **5**, 27–36 (2015).
- Nobre, C. A. et al. Land-use and climate change risks in the Amazon and the need of a novel sustainable development paradigm. *Proc. Natl Acad. Sci.* **113**, 10759–10768 (2016).
- Leite-Filho, A. T., Soares-Filho, B. S., Davis, J. L., Abrahão, G. M. & Börner, J. Deforestation reduces rainfall and agricultural revenues in the Brazilian Amazon. *Nat. Commun.* **12**, 1–7 (2021).
- Hubau, W. et al. Asynchronous carbon sink saturation in African and Amazonian tropical forests. *Nature* **579**, 80–87 (2020).
- Brienen, R. J. W. et al. Long-term decline of the Amazon carbon sink. *Nature* **519**, 344–348 (2015).
- Doughty, C. E. et al. Drought impact on forest carbon dynamics and fluxes in Amazonia. *Nature* **519**, 78–82 (2015).
- Doughty, C. E. et al. Tropical forests are approaching critical temperature thresholds. *Nature* 1–7. <https://doi.org/10.1038/s41586-023-06391-z> (2023).
- Fawcett, D. et al. Declining Amazon biomass due to deforestation and subsequent degradation losses exceeding gains. *Glob. Change Biol.* **29**, 1106–1118 (2022).
- Silva Junior, C. H. L. et al. The Brazilian Amazon deforestation rate in 2020 is the greatest of the decade. *Nat. Ecol. Evol.* **5**, 144–145 (2021).
- Kruid, S. et al. Beyond deforestation: carbon emissions from land grabbing and forest degradation in the Brazilian Amazon. *Front. Forests Glob. Change* **4** (2021).
- Qin, Y. et al. Carbon loss from forest degradation exceeds that from deforestation in the Brazilian Amazon. *Nat. Clim. Change* **11**, 442–448 (2021).
- Matricardi, E. A. T. et al. Long-term forest degradation surpasses deforestation in the Brazilian Amazon. *Science* **369**, 1378–1382 (2020).
- Aragão, L. E. O. C. et al. 21st Century drought-related fires counteract the decline of Amazon deforestation carbon emissions. *Nat. Commun.* **9**, 1–12 (2018).
- Bullock, E. L., Woodcock, C. E., Souza, C. & Olofsson, P. Satellite-based estimates reveal widespread forest degradation in the Amazon. *Glob. Change Biol.* **26**, 2956–2969 (2020).

19. Lapola, D. M. et al. The drivers and impacts of Amazon forest degradation. *Science* **379**, eabp8622 (2023).
20. Heinrich, V. H. A. et al. Large carbon sink potential of secondary forests in the Brazilian Amazon to mitigate climate change. *Nat. Commun.* **12**, 1–11 (2021).
21. Silva, C. V. J. et al. Estimating the multi-decadal carbon deficit of burned Amazonian forests. *Environ. Res. Lett.* **15** (2020).
22. Silva Junior, C. H. L. et al. Persistent collapse of biomass in Amazonian forest edges following deforestation leads to unaccounted carbon losses. *Sci. Adv.* **6**, eaaz8360 (2020).
23. Sitch, S. et al. Recent trends and drivers of regional sources and sinks of carbon dioxide. *Biogeosciences* **12**, 653–679 (2015).
24. Houghton, R. A. & Nassikas, A. A. Global and regional fluxes of carbon from land use and land cover change 1850–2015. *Glob. Biogeochem. Cycles* **31**, 456–472 (2017).
25. Hansis, E., Davis, S. J. & Pongratz, J. Relevance of methodological choices for accounting of land use change carbon fluxes. *Glob. Biogeochem. Cycles* **29**, 1230–1246 (2015).
26. Aguiar, A. P. D. et al. Modeling the spatial and temporal heterogeneity of deforestation-driven carbon emissions: The INPE-EM framework applied to the Brazilian Amazon. *Glob. Change Biol.* **18**, 3346–3366 (2012).
27. Harris, N. L. et al. Global maps of twenty-first century forest carbon fluxes. *Nat. Clim. Change* **11**, 234–240 (2021).
28. Peylin, P. et al. *Global Atmospheric Carbon Budget: Results from an Ensemble of Atmospheric CO<sub>2</sub> Inversions*. <https://bg.copernicus.org/preprints/10/5301/2013/bgd-10-5301-2013.pdf> (2013).
29. Kondo, M. et al. State of the science in reconciling top-down and bottom-up approaches for terrestrial CO<sub>2</sub> budget. *Glob. Change Biol.* **26**, 1068–1084 (2020).
30. Assis, T. O. et al. CO<sub>2</sub> emissions from forest degradation in Brazilian Amazon. *Environ. Res. Lett.* **15**, 104035 (2020).
31. Tejada, G. et al. CO<sub>2</sub> emissions in the Amazon: are bottom-up estimates from land use and cover datasets consistent with top-down estimates based on atmospheric measurements? *Front. Forests Glob. Change* **6** (2023).
32. Gatti, L. V. et al. Amazonia as a carbon source linked to deforestation and climate change. *Nature* **595**, 388–393 (2021).
33. Aragão, L. E. O. C. et al. Environmental change and the carbon balance of Amazonian forests. *Biol. Rev.* **89**, 913–931 (2014).
34. Hansen, M. C. et al. High-resolution global maps of 21st-century forest cover change. *Science* **342**, 850–853 (2013).
35. McDowell, N. et al. Drivers and mechanisms of tree mortality in moist tropical forests. *N. Phytol.* **219**, 851–869 (2018).
36. Rosan, T. M. et al. A multi-data assessment of land use and land cover emissions from Brazil during 2000–2019. *Environ. Res. Lett.* **16**, 074004 (2021).
37. Albert, J. et al. The multiple viewpoints for the Amazon: geographic limits and meanings. [https://www.theamazonwewant.org/wp-content/uploads/2021/09/220105\\_The-multiple-viewpoints-for-the-Amazon-formatted-and-reviewed-050122.pdf](https://www.theamazonwewant.org/wp-content/uploads/2021/09/220105_The-multiple-viewpoints-for-the-Amazon-formatted-and-reviewed-050122.pdf) (2021).
38. Basso, L. S. et al. Atmospheric CO<sub>2</sub> inversion reveals the Amazon as a minor carbon source caused by fire emissions, with forest uptake offsetting about half of these emissions. *Atmos. Chem. Phys.* **23**, 9685–9723 (2023).
39. Friedlingstein, P. et al. Global Carbon Budget 2022. *Earth Syst. Sci. Data* **14**, 4811–4900 (2022).
40. Van Der Werf, G. R. et al. Global fire emissions estimates during 1997–2016. *Earth Syst. Sci. Data* **9**, 697–720 (2017).
41. Bloom, A. A. & Williams, M. Constraining ecosystem carbon dynamics in a data-limited world: integrating ecological ‘common sense’ in a model–data fusion framework. *Biogeosciences* **12**, 1299–1315 (2015).
42. Bloom, A. A., Exbrayat, J.-F., van der Velde, I. R., Feng, L. & Williams, M. The decadal state of the terrestrial carbon cycle: Global retrievals of terrestrial carbon allocation, pools, and residence times. *Proc. Natl Acad. Sci.* **113**, 1285–1290 (2016).
43. Aragão, L. E. O. C. et al. Spatial patterns and fire response of recent Amazonian droughts. *Geophys. Res. Lett.* **34** (2007).
44. Phillips, O. L. et al. Carbon uptake by mature Amazon forests has mitigated Amazon nations’ carbon emissions. *Carbon Balance Manag.* **12**, 1–9 (2017).
45. INPE. Emissões líquidas com degradação. *Inpe-EM* <http://inpe-em.ccst.inpe.br/emissoes-liquidas-com-degracao-amz/>.
46. Giglio, L., Boschetti, L., Roy, D. P., Humber, M. L. & Justice, C. O. The Collection 6 MODIS burned area mapping algorithm and product. *Remote Sensing Environ.* **217**, 72–85 (2018).
47. Barlow, J., Berenguer, E., Carmenta, R. & França, F. Clarifying Amazonia’s burning crisis. *Glob. Change Biol.* **26**, 319–321 (2020).
48. Gatti, L. V. et al. Increased Amazon carbon emissions mainly from decline in law enforcement. *Nature* 1–6. <https://doi.org/10.1038/s41586-023-06390-0> (2023).
49. Trancoso, R. Changing Amazon deforestation patterns: Urgent need to restore command and control policies and market interventions. *Environ. Res. Lett.* **16** (2021).
50. West, T. A. P. & Fearnside, P. M. Brazil’s conservation reform and the reduction of deforestation in Amazonia. *Land Use Policy* **100**, 105072 (2021).
51. Friedlingstein, P. et al. Global Carbon Budget 2021. 1917–2005 (2022).
52. Alencar, A. A. C. et al. Long-term landsat-based monthly burned area dataset for the Brazilian biomes using deep learning. *Remote Sensing* **14**, 2510 (2022).
53. O’Sullivan, M. et al. Process-oriented analysis of dominant sources of uncertainty in the land carbon sink. *Nat. Commun.* **13**, 4781 (2022).
54. Parry, I. M., Ritchie, P. D. L. & Cox, P. M. Evidence of localised Amazon rainforest dieback in CMIP6 models. *Earth Syst. Dyn.* **13**, 1667–1675 (2022).
55. Ritchie, P. D. L., Parry, I., Clarke, J. J., Huntingford, C. & Cox, P. M. Increases in the temperature seasonal cycle indicate long-term drying trends in Amazonia. *Commun. Earth Environ.* **3**, 1–8 (2022).
56. Parsons, L. A. Implications of CMIP6 Projected Drying Trends for 21st Century Amazonian Drought Risk. *Earth’s Future* **8**, e2020EF001608 (2020).
57. Anderegg, W. R. L. & Venturas, M. D. Plant hydraulics play a critical role in Earth system fluxes. *N. Phytol.* **226**, 1535–1538 (2020).
58. Staal, A. et al. Feedback between drought and deforestation in the Amazon. *Environ. Res. Lett.* **15** (2020).
59. Barkhordarian, A., Saatchi, S. S., Behrangi, A., Loikith, P. C. & Mechoso, C. R. A recent systematic increase in vapor pressure deficit over tropical South America. *Sci. Rep.* **9**, 1–12 (2019).
60. Boulton, C. A., Lenton, T. M. & Boers, N. Pronounced loss of Amazon rainforest resilience since the early 2000s. *Nat. Clim. Change* **12** (2022).
61. Houghton, R. A. Why are estimates of the terrestrial carbon balance so different? *Glob. Change Biol.* **9**, 500–509 (2003).
62. Houghton, R. A. et al. Annual fluxes of carbon from deforestation and regrowth in the Brazilian Amazon. *Nature* **403**, 301–304 (2000).
63. de Almeida, C. A. et al. High spatial resolution land use and land cover mapping of the Brazilian Legal Amazon in 2008 using Landsat-5/TM and MODIS data. *Acta Amazonica* **46**, 291–302 (2016).
64. Almeida, C. A. Estimativa da área e do tempo de permanência da vegetação secundária na Amazônia Legal por meio de imagens Landsat/TM. *Sensoriamento Remoto Mestrado*, 130 (2009).
65. Houghton, R. A. Revised estimates of the annual net flux of carbon to the atmosphere from changes in land use and land management 1850–2000. *Tellus, Ser. B: Chem. Phys. Meteorol.* **55**, 378–390 (2003).
66. Chini, L. et al. Land-use harmonization datasets for annual global carbon budgets. *Earth Syst. Sci. Data* **13**, 4175–4189 (2021).
67. Hurtt, G. et al. Harmonization of Global Land-Use Change and Management for the Period 850–2100 (LUH2) for CMIP6. *Geosci. Model Dev. Discussions* 1–65 <https://doi.org/10.5194/gmd-2019-360> (2020).
68. Goldewijk, K. K., Beusen, A., Doelman, J. & Stehfest, E. Anthropogenic land use estimates for the Holocene - HYDE 3.2. *Earth Syst. Sci. Data* **9**, 927–953 (2017).
69. Novaes, R. M. L. et al. Brazil’s agricultural land, cropping statistics and new estimates (2022).
70. Brazil MCTI. Fourth national communication of Brazil to the united nations framework convention on climate change (2020).
71. Obermeier, W. A. et al. Modelled land use and land cover change emissions—a spatio-temporal comparison of different approaches. *Earth Syst. Dyn.* **12**, 635–670 (2021).
72. Harris, I., Osborn, T. J., Jones, P. & Lister, D. Version 4 of the CRU TS monthly high-resolution gridded multivariate climate dataset. *Sci Data* **7**, 109 (2020).
73. Harris, I., Jones, P. D., Osborn, T. J. & Lister, D. H. Updated high-resolution grids of monthly climatic observations—the CRU TS3.10 Dataset. *Int. J. Climatol.* **34**, 623–642 (2014).
74. Kobayashi, S. et al. The JRA-55 reanalysis: general specifications and basic characteristics. *J. Meteorol. Soc. Japan. Ser. II* **93**, 5–48 (2015).
75. Gibbs, H. K., Brown, S., Niles, J. O. & Foley, J. A. Monitoring and estimating tropical forest carbon stocks: making REDD a reality. *Environ. Res. Lett.* **2**, 045023 (2007).
76. Chipperfield, M. P. New version of the TOMCAT/SLIMCAT off-line chemical transport model: Intercomparison of stratospheric tracer experiments. *Q. J. Roy. Meteorol. Soc.* **132**, 1179–1203 (2006).
77. Wilson, C., Chipperfield, M. P., Gloor, M. & Chevallier, F. Development of a variational flux inversion system (INVICAT v1.0) using the TOMCAT chemical transport model. *Geosci. Model Dev.* **7**, 2485–2500 (2014).
78. Gloor, E. et al. Tropical land carbon cycle responses to 2015/16 El Niño as recorded by atmospheric greenhouse gas and remote sensing data. *Phil. Trans. Roy. Soc. B: Biol. Sci.* **373**, 20170302 (2018).
79. Takahashi, T. et al. Climatological mean and decadal change in surface ocean pCO<sub>2</sub>, and net sea–air CO<sub>2</sub> flux over the global oceans. *Deep Sea Res. Part II: Top. Stud. Oceanogr.* **56**, 554–577 (2009).
80. Khattiwala, S., Primeau, F. & Hall, T. Reconstruction of the history of anthropogenic CO<sub>2</sub> concentrations in the ocean. *Nature* **462**, 346–349 (2009).
81. Gatti, L. V. et al. Drought sensitivity of Amazonian carbon balance revealed by atmospheric measurements. *Nature* **506**, 76–80 (2014).

82. Haario, H., Saksman, E. & Tamminen, J. An adaptive Metropolis algorithm. *Bernoulli* **7**, 223–242 (2001).
83. Williams, M., Schwarz, P. A., Law, B. E., Irvine, J. & Kurpius, M. R. An improved analysis of forest carbon dynamics using data assimilation. *Glob. Change Biol.* **11**, 89–105 (2005).

## Acknowledgements

The development of this research has been supported by the Newton Fund through the Met Office Climate Science for Service Partnership Brazil (CSSP Brazil), RECCAP2 project which is part of the ESA Climate Change Initiative (contract no. 4000123002/18/I-NB), and the H2020 European Institute of Innovation and Technology (4C; Grant No. 821003). C.W. is funded via UK National Centre for Earth Observation (NE/R016518/1 and NE/N018079/1). L.S.B. is funded by State of Sao Paulo Science Foundation—FAPESP (2018/14006-4, 2020/02656-4). L.G. was funded by CARBAM project (FAPESP 2016/02018-2). ORNL is managed by UT-Battelle, LLC, for the DOE under contract DE-AC05-1008 00OR22725. For the purpose of open access, the author has applied a 'Creative Commons Attribution (CC BY) licence to any Author Accepted Manuscript version arising. We thank Ian Harris for advising us on the CRUJRA forcing dataset.

## Author contributions

T.M.R., S.S., E.G., and L.E.O.C.A. designed the study. T.M.R., M.O.S., L.S.B., C.W., C.S. compiled the data. TMR conducted all the data analysis with inputs from J.G.S., V.H., and D.F. T.M.R. and S.S. led the writing of the manuscript to which all co-authors contributed with comments and inputs. J.P. and C.I.S. provided the BLUE bookkeeping model. A.A., V.K.A., S.F., A.K.J., E.K., D.K., J.K., M.O.S., B.P., Q.S., H.T., A.P.W., W.Y., X.Y., and S.Z. provided the dynamic global vegetation models, with synthesis by TMR and MOS. L.S.B., C.W., and E.G. provided the atmospheric inversion. C.S. provided the net fluxes of fire degradation (FATE) in the Brazilian Amazon. F.G.S.B. and C.v.R. provided the INPE-EM data. MW and LS provided the CARDAMOM net biome productivity data.

## Competing interests

The authors declare no competing interests.

## Additional information

**Supplementary information** The online version contains supplementary material available at <https://doi.org/10.1038/s43247-024-01205-0>.

**Correspondence** and requests for materials should be addressed to Thais M. Rosan.

**Peer review information** *Communications Earth & Environment* thanks the anonymous reviewers for their contribution to the peer review of this work. Primary Handling Editors: Yongqiang Liu and Clare Davis. A peer review file is available.

**Reprints and permission information** is available at <http://www.nature.com/reprints>

**Publisher's note** Springer Nature remains neutral with regard to jurisdictional claims in published maps and institutional affiliations.



**Open Access** This article is licensed under a Creative Commons Attribution 4.0 International License, which permits use, sharing, adaptation, distribution and reproduction in any medium or format, as long as you give appropriate credit to the original author(s) and the source, provide a link to the Creative Commons licence, and indicate if changes were made. The images or other third party material in this article are included in the article's Creative Commons licence, unless indicated otherwise in a credit line to the material. If material is not included in the article's Creative Commons licence and your intended use is not permitted by statutory regulation or exceeds the permitted use, you will need to obtain permission directly from the copyright holder. To view a copy of this licence, visit <http://creativecommons.org/licenses/by/4.0/>.

© The Author(s) 2024

<sup>1</sup>Faculty of Environment, Science and Economy, University of Exeter, Exeter, UK. <sup>2</sup>School of Geography, University of Leeds, Leeds LS2 9JT, UK. <sup>3</sup>General Coordination of Earth Science (CGCT), National Institute for Space Research (INPE), São José dos Campos, Brazil. <sup>4</sup>National Centre for Earth Observation, University of Leeds, Leeds, UK. <sup>5</sup>School of Earth and Environment, University of Leeds, Leeds, UK. <sup>6</sup>Instituto de Pesquisas Ambientais da Amazônia, Brasília, DF, Brazil. <sup>7</sup>Lancaster Environment Centre, Lancaster University, Lancaster, UK. <sup>8</sup>BeZero Carbon Ltd, London, UK. <sup>9</sup>Swiss Federal Institute for Forest Snow and Landscape Research WSL, Birmensdorf, Switzerland. <sup>10</sup>UK Centre for Ecology & Hydrology, Wallingford OX10 8BB, UK. <sup>11</sup>Met Office Hadley Centre, Exeter, UK. <sup>12</sup>Department of Geography, Ludwig-Maximilians-Universität München (LMU), Munich, Germany. <sup>13</sup>Max Planck Institute for Meteorology, Hamburg, Germany. <sup>14</sup>School of GeoSciences and National Centre for Earth Observation, University of Edinburgh, Edinburgh EH9 3FF, UK. <sup>15</sup>Hawkesbury Institute for the Environment, Western Sydney University, Penrith, NSW, Australia. <sup>16</sup>Canadian Centre for Climate Modelling and Analysis, Climate Research Division, Environment and Climate Change Canada, Victoria, BC, Canada. <sup>17</sup>National Center for Atmospheric Research, Climate and Global Dynamics, Terrestrial Sciences Section, Boulder, CO 80305, USA. <sup>18</sup>Schiller Institute for Integrated Science and Society, Department of Earth and Environmental Sciences, Boston College, Chestnut Hill, MA 02467, USA. <sup>19</sup>School of Atmospheric Sciences, Southern Marine Science and Engineering Guangdong Laboratory (Zhuhai), Sun Yat-sen University, 519082 Zhuhai, Guangdong, China. <sup>20</sup>Department of Atmospheric Sciences, University of Illinois, Urbana-Champaign, IL 61801, USA. <sup>21</sup>NASA Goddard Space Flight Center, Biospheric Sciences Lab., Greenbelt, MD 20771, USA. <sup>22</sup>Karlsruhe Institute of Technology, Institute of Meteorology and Climate Research/Atmospheric Environmental Research, 82467 Garmisch-Partenkirchen, Germany. <sup>23</sup>Climate and Environmental Physics, Physics Institute and Oeschger Centre for Climate Change Research, University of Bern, Bern, Switzerland. <sup>24</sup>Max Planck Institute for Biogeochemistry, P.O. Box 600164 Hans-Knöll-Str. 10, 07745 Jena, Germany. <sup>25</sup>Environmental Sciences Division and Climate Change Science Institute, Oak Ridge National Laboratory, Oak Ridge, TN 37831, USA. <sup>26</sup>Institute of Applied Energy (IAE), Minato-ku, Tokyo 105-0003, Japan. <sup>27</sup>School of Environmental Science and Engineering, Nanjing University of Information Science and Technology (NUIST), 211544 Nanjing, China. <sup>28</sup>Laboratoire des Sciences du Climat et de l'Environnement, LSCE/IPSL, CEA-CNRS-UVSQ, Université Paris-Saclay, 91191 Gif-Sur-Yvette, France. <sup>29</sup>ISPA, INRAE Bordeaux, 33140 Villenave d'Ornon, France. <sup>30</sup>European Space Agency Climate Office, ECSAT, Harwell Campus, Didcot, UK. <sup>✉</sup>email: [T.Rosan@exeter.ac.uk](mailto:T.Rosan@exeter.ac.uk)